LO-09-001

Determining Off-Normal Solar Optical Properties of Drapery Fabrics

Nathan Kotey, PhD
Student Member ASHRAE

John L. Wright, PhD, PEng
Member ASHRAE

Michael Collins, PhD, PEng
Associate Member ASHRAE

ABSTRACT

The determination of off-normal solar optical properties of drapery fabrics is particularly useful in modelling the effective solar optical properties of pleated drapery. Special sample holders were designed and fabricated to facilitate measurements using an integrating sphere installed in a commercially available spectrophotometer. Measurements were taken for eight of the nine fabric designations documented in the ASHRAE Handbook – Fundamentals. Measurements were also obtained for a sheer fabric which does not fall into any of the customary fabric designations. Semi-empirical models were developed to quantify the variation of solar optical properties with respect to incidence angle. Given solar optical properties obtained at normal incidence, these models can be used to characterise the off-normal beam-beam and beam-diffuse properties of a drapery fabric. The fabric models comprise a useful component of pleated drapery models and, in turn, a valuable tool for building energy simulation. The measurement technique described in this study can be used to obtain the off-normal solar optical properties of additional flat shading devices such as roller blinds and insect screens.

INTRODUCTION

Solar gain is known to offset heating load but also manifests itself as increased peak cooling load and increased cooling energy consumption. The use of shading devices to control solar gain through windows is an important research topic. This is largely true because shading devices such as venetian blinds, roller blinds and draperies offer a cost effective strategy to actively accept or reject solar gain. Solar gain can be accepted when heating is required and rejected otherwise. The ability to control solar gain is especially important for the successful operation of well insulated, energy efficient buildings.

The influence of shading devices can be calculated when optical and thermal properties of the individual glazing/shading layers are known. The procedure takes advantage of the fact that there is no appreciable overlap between the solar and longwave radiation bands. This leads to a two-step analysis. First, solar radiation models determine the fraction of incident solar radiation directly transmitted and the fraction that is absorbed in each layer. The absorbed solar radiation in each layer then serves as a source term in the second step – the heat transfer analysis. A building energy simulation might include this analysis in an hour-by-hour calculation. Since the location of the sun and the incidence angle change by the hour, the solar optical properties of the individual layers must be available at any given incidence and/or profile angle.

The off-normal solar properties of clear and tinted glass can readily be determined (e.g., Pettit 1979, Furler 1991). Several models have also been devised to characterize coated glass (e.g., Pfrommer et al. 1995, Roos 1997, Rubin et al. 1998, Rubin et. al. 1999).

In general, shading layers may be characterized by making the assumption that each layer, whether homogeneous or not, can be represented by an equivalent homogenous layer that is assigned spatially-averaged "effective" optical properties. This approach has been used in a number of studies (e.g., Parmelee and Aubele 1952, Farber et al. 1963, Pfrommer et al. 1996, van Dijk et al. 2002, Yahoda and Wright 2005) and has been shown to provide accurate characterization of venetian blinds (e.g., Kotey et al. 2008).

When solar radiation is incident on a shading layer, some portion of the radiation passes undisturbed through openings

Nathan Kotey is a graduate student, **John Wright** is a professor, and **Michael Collins** is an associate professor in the Department of Mechanical and Mechatronics Engineering, University of Waterloo, Waterloo, Ontario, CA.

in the layer and the remaining portion is intercepted by the structure of the layer. The structure may consist of yarn, slats, or some other material. The portion of the intercepted radiation that is not absorbed will be scattered and will leave the layer as an apparent reflection or transmission. These scattered components are assumed to be uniformly diffuse. In addition, a shading layer will generally transmit longwave radiation (i.e., it is diathermanous), by virtue of its openness, and effective longwave properties are assigned accordingly.

Using effective optical properties and a beam/diffuse split of solar radiation at each layer, the framework used to represent multi-layer systems (Wright and Kotey 2006, Wright 2008) provides virtually unlimited freedom to consider different types of shading layers. This framework also delivers the computational speed needed in the context of building energy simulation.

Techniques for characterising the off-normal properties of fabrics and pleated draperies are not readily available (e.g., Keyes 1967, Kotey et al. 2007). The most widely used information originated with Keyes (1967) who used visual inspection to characterise fabrics by yarn colour (yarn reflectance) as dark (D), medium (M) and light (L) and by weave as open (I), semi-open (II) and closed (III). The yarn reflectance and openness factor of fabrics were conveniently represented on a chart allowing the user to estimate the shading effect of a pleated drape. Using fabric transmittance and reflectance as independent variables, a similar chart was generated by Moore and Pennington (1967). Keyes (1967) then reconciled the two charts. Keyes (1967) universal chart, shown in Figure 1, is the basis of the interior attenuation coefficient (IAC) values that apply to glass-drapery combinations found in ASHRAE Handbook-Fundamentals (2005). This chart offers the possibility of using measured (beam-total transmittance and beam-total reflectance at normal incidence) or eye-observed optical properties (openness and yarn colour) to estimate the shading effect of pleated draperies with 100% fullness.

More recently, Hunn et al. (1991) designed an apparatus to measure the bidirectional transmittance and reflectance distribution of fabrics. The measurements revealed the effect of textile properties (openness of weave, fibre cross section and fabric structure) on the distribution of sunlight. Such information is particularly useful in the context of daylighting simulation. Bidirectional solar optical properties can be incorporated into matrix layer calculation methods (e.g., Klems 1994a and 1994b) to predict the solar gain of glazing/shading systems. However, this experimental method and the associated glazing/shading system layer system analysis are not well suited to building energy simulation because of their complexity and because of the significant amount of CPU time required.

The techniques that might be used to measure the off-normal solar optical properties of glazings cannot be applied to fabrics. This is due to the fact that fabric surfaces are rough and scatter incident radiation. Nevertheless, the existing tech-

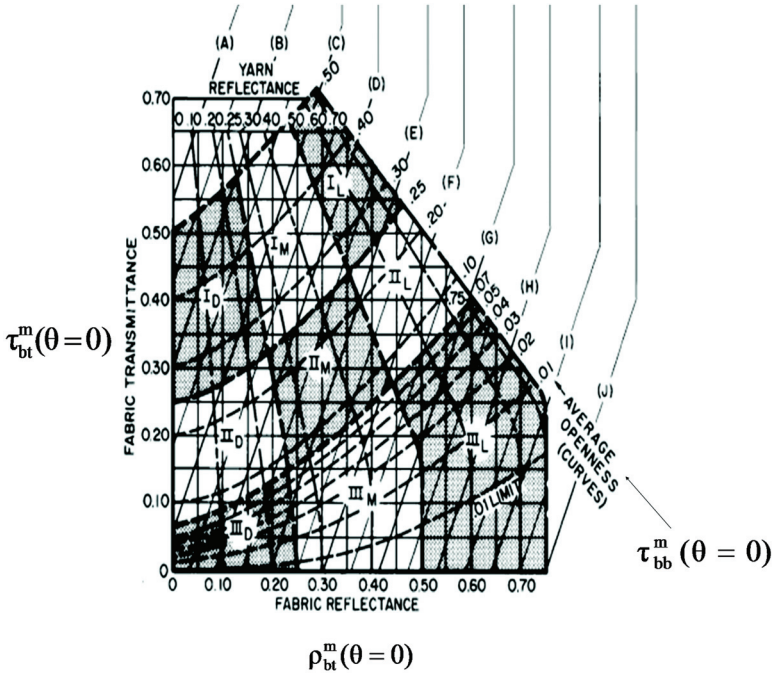

Figure 1 *Keyes Universal Chart (adopted from ASHRAE 2005).*

niques can be adapted. To achieve this, special sample holders were designed and fabricated to facilitate the measurement of off-normal solar optical properties of fabrics using an integrating sphere installed in a commercially available spectrophotometer. The integrating sphere is particularly useful because it can resolve the undisturbed and scattered components of transmitted or reflected beam radiation. The sample holders were made from polished aluminium tubes with one end truncated at a known angle, θ. The interior surface of each tube was painted black in order to absorb radiation scattered in reflection during a transmittance measurement or scattered in transmission during a reflectance measurement. A similar technique was used by Pettit (1979) to measure the off-normal transmittance of glazings. Pettit's measurements compared favourably with results obtained from first principles.

In the current study, spectral measurements of beam-beam transmittance, beam-diffuse transmittance and beam-diffuse reflectance were obtained at incidence angles, θ, ranging from 0 to 60°. These data showed that fabrics are generally not spectrally selective except for variation in the visible region corresponding to the colour of the fabric. Since the aim of the current study was to generate solar (spectral-averaged) optical properties for building energy simulation, no spectral data are presented. The solar optical properties were calculated using the 50-point selected ordinate method as described in ASTM E903-96 (1996). A second procedure was devised to repeat the beam-beam transmittance measurements, this time without the integrating sphere and at incidence angle as high as 80°. Having two sets of beam-beam transmission data offered an opportunity to compare and gain confidence in the new procedures.

The direct measurement of off-normal solar optical properties of all drapery fabrics on the market is not a practical option. A realistic approach is to develop models that require a small number of readily obtained measurements as input. Such an approach was used in determining the off-normal solar optical properties of coated and tinted glazings (e.g., Furler 1991, Roos 1997, Karlsson and Roos 2000). The models developed in this study can be applied as long as the user knows where the fabric is located on Keyes' chart (Figure 1).

OBJECTIVES AND APPROACH

The main objective of the current research was to develop semi-empirical models for off-normal solar optical properties of drapery fabrics. This objective was achieved by measuring the off-normal solar optical properties of a wide variety of fabric samples using special sample holders attached to an integrating sphere.

A simple but pragmatic way to characterize fabrics is to assume that normalized transmittance and reflectance data share a common functional dependence with respect to incidence angle. In this study a cosine power function was chosen to represent this dependence. This was done for several reasons, including simplicity. The cosine function is symmetrical, having zero gradient at $\theta = 0$ (normal incidence). It has maximum and minimum values at $\theta = 0$ and at $\theta = 90°$. Also, the shape of the curve can be modified by changing the value of the exponent. Each model component was tuned using a set of integrating sphere measurements and, although the formulation appears to be primarily empirical, an effort was made to incorporate known or expected trends and limiting cases in order to make the resulting models as general and reliable as possible.

PRELIMINARY CONSIDERATIONS

Fabrics consist of strands of yarn that are woven or knitted. The yarn itself is made up of fibres that are twisted and plied. Strands of yarn can be woven loosely, leaving open areas, or woven tightly with little or no open area. Furthermore, strands of yarn that are loosely twisted and plied could have open areas between the fibres. Fabrics may be classified by weave as open, semi-open and closed. The colour of the yarn may be used to classify fabrics as light, medium or dark. See Figure 1.

A portion of incident beam radiation will pass undisturbed through the openings of the fabric. The remaining portion encounters the structure of the fabric and undergoes multiple reflections between the fibres as well as possible transmission through the fibres. The portion of the intercepted radiation that is not absorbed by the fibres emerges in the forward or backward direction (Keyes 1967). The undisturbed radiation transmitted through the openings constitutes the beam-beam transmittance (specular transmittance), τ_{bb}^{m}. The superscript "m" is used to denote a property of a fabric (i.e., a material). At normal incidence the beam-beam transmittance is equivalent to the openness factor (Keyes 1967), $A_o = \tau_{bb}^{m}(\theta = 0)$, which is defined as the ratio of the open area to the total area of the fabric. The portion of intercepted/scattered radiation that emerges in the forward direction constitutes beam-diffuse transmittance, τ_{bd}^{m}, while the portion that emerges in the backward direction is the beam-diffuse reflectance, ρ_{bd}^{m}. These scattered components are assumed to be uniformly diffuse. The beam-total transmittance (directional-hemispherical transmittance), τ_{bt}^{m}, is the sum of τ_{bb}^{m} and τ_{bd}^{m}. It was assumed that fabrics do not exhibit specular reflection, $\rho_{bb}^{m} \approx 0$, and this was confirmed experimentally. The beam-total reflectance (directional-hemispherical reflectance), ρ_{bd}^{m}, is therefore equal to the beam-diffuse reflectance, $\rho_{bt}^{m} = \rho_{bd}^{m}$. Accordingly, incident diffuse radiation is also assumed to be transmitted and reflected diffusely by the fabric. The corresponding diffuse-diffuse properties are τ_{dd}^{m} and ρ_{dd}^{m}.

MEASUREMENT TECHNIQUE

Spectrophotometer

The spectrophotometer used in this study is a double beam, direct ratio recording, rapid scanning instrument. It has a resolution of less than 0.05 nm for the ultraviolet and visible spectra (UV-VIS) and less than 0.2 nm for the near infrared

spectrum (NIR); a repeatability characteristic of less than 0.025 nm for UV-VIS and less than 0.1 nm for NIR. In operation, two detectors, a Photomultiplier Tube (PMT) and a lead-sulphide (PbS) photoconductive sensor, are illuminated alternately by the sample and the reference beam. The PMT is used in the wavelength range of $0.17 < \lambda < 0.8\mu m$ and the PbS detector responds in the $0.8 < \lambda < 3.3\mu m$ wavelength range. There are a several accessories that can be attached to the spectrophotometer. For the purpose of the current investigation the spectrophotometer was operated, in most cases, with the integrating sphere attachment.

Integrating Sphere

Integrating spheres are designed to measure, and distinguish between, beam and scattered components of transmitted and reflected radiation. Light enters the sphere through a port and reflection from the interior surface must be purely diffuse. Light inside the sphere becomes uniformly distributed over the entire inner surface, eliminating any directional or spatial non-uniformity of the incoming radiation, and detectors measure this integrated signal. The detector signal is proportional to the rate at which radiant energy enters at the inlet port and the ratio between the two is called the "response of the sphere". The surface of the sphere must be very highly reflective to maximize the response of the sphere and produce a signal that can be accurately detected. Theory and operating principles can be found in many references (e.g., Edwards et al. 1961, Lovell 1984).

A 110 mm (4.33 in.) diameter sphere with a polytetrafluoroethylene (PTFE) coating was used in this study. The detectors are mounted at the top and are shielded by baffles so that they view only the bottom wall of the sphere. The operational range of the detectors is $0.17 < \lambda < 3.3\mu m$ but the spectral reflectance characteristic of the PTFE restricts useful measurements to the range of $0.25 < \lambda < 2.5\mu m$. Nonetheless, this more limited wavelength range includes almost 98% of the solar spectrum. This particular apparatus was designed for making measurements with incident radiation normal to the surface of the test sample.

Transmittance can be measured by mounting a sample at the transmission port. See Figure 2. Reference measurements of the zero and full transmission extremes are made for calibration. The latter, called the 100% baseline, is obtained with the sample removed while a fixture is inserted at the reflection port to complete the sphere. The 0% baseline is measured with the transmission port blocked. The beam-diffuse transmittance is measured with the sample in place and the reflection port open, allowing the transmitted beam component to escape while trapping the scattered radiation, as shown in Figure 2a. The beam-total (beam-beam plus beam-diffuse) transmittance is measured with the reflection port covered. See Figure 2b. The beam-beam transmittance is the difference between the two readings.

To measure reflectance radiation is allowed to enter the sphere through the open transmission port and samples are placed at the reflection port. See Figure 3. The full-scale baseline is obtained by covering the reflection port with a sample of known reflectance. This reference sample reflects incident radiation diffusely into the sphere. The 0% baseline is measured with the reflection port open, allowing the beam to escape. The test sample is then mounted at the reflection port and radiation reflected from the sample is collected by the sphere. The reflection port has a movable positioning cap. To measure the beam-diffuse component the cap is mounted as shown in Figure 3a, allowing the incident beam to strike the sample at $\theta = 0$ and causing the beam-beam reflection compo-

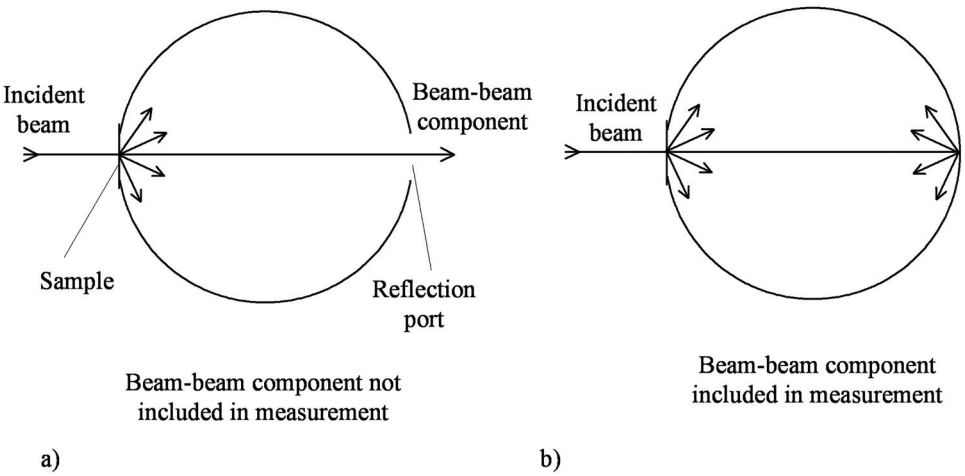

Figure 2 *a) Beam-diffuse transmittance measurement; b) Beam-total transmittance measurement.*

nent to exit through the transmission port. When the cap is mounted as shown in Figure 3b, $\theta \approx 3°$, both components remain in the sphere and the detectors measure beam-total reflectance. Again, the beam-beam reflectance is simply the difference between the two readings.

Fixed Sample Holders

Sample holders were designed and fabricated to adapt the integrating sphere for measurement of transmittance and reflectance at off-normal incidence. The sample holders were made from aluminium tubes with one end truncated at an angle, θ, with θ ranging from 0 to 60° in 15° steps. Adapters were also built to mount sample holders at the reflection or transmission port. Figure 4 shows a set of sample holders and the two adapters. Each sample holder is 40 mm (1.57 in.) long with internal and external diameters of 13.75 and 15.75 mm. (0.54 and 0.62 in.). At the transmission port, the incident beam is rectangular in cross-section with dimensions of 13.44 mm x 11.04 mm. (0.53 in. x 0.43 in.). Thus, the diagonal of the beam cross-section is 17.39 mm (0.68 in.) which is greater than the internal diameter of the holder. To ensure that the incident beam would pass through the holder without interference a beam reducer was glued to the outer face of the transmission port adapter. The beam reducer is simply a thin plate with a 12.80 mm (0.50 in.) diameter hole.

When installed, a fixed sample holder projects into the integrating sphere. Its exterior surface was highly polished to reflect radiation and to avoid degrading the response of the sphere.

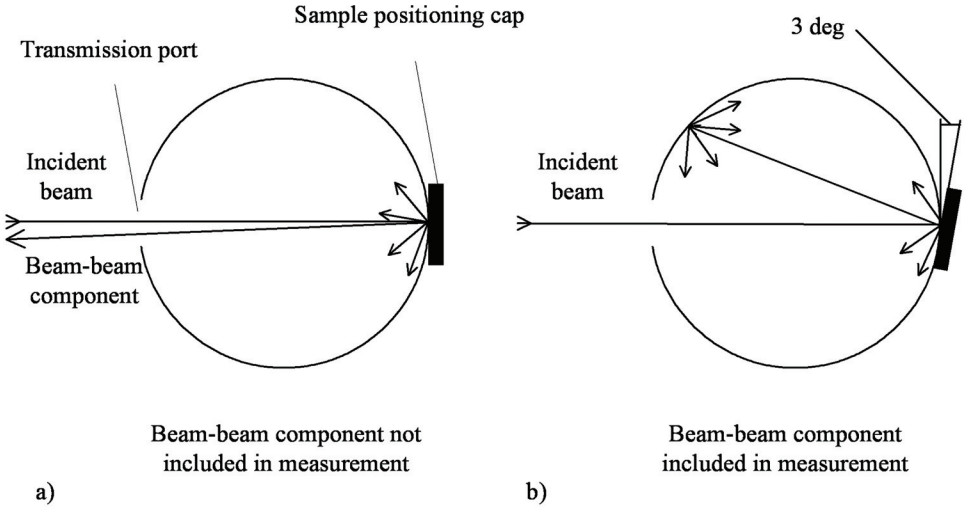

Figure 3 *a) Beam-diffuse reflectance measurement; b) Beam-total reflectance measurement.*

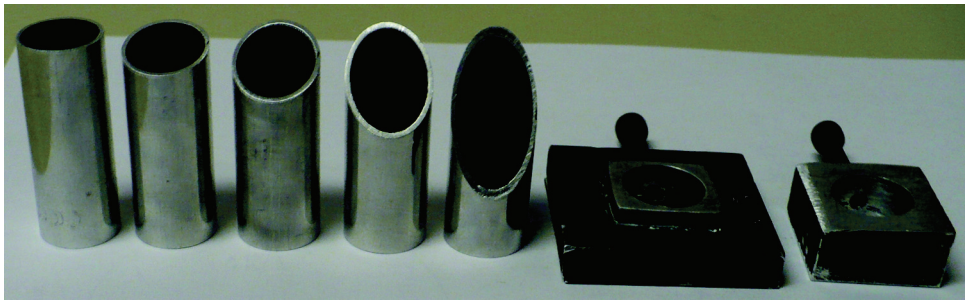

Figure 4 *A set of fixed sample holders, transmission and reflection adapters.*

The interior surface of each sample holder was painted black to absorb radiation scattered in reflection during a transmittance measurement or scattered in transmission during a reflectance measurement.

A set of reflectance references was also fabricated. They were made by filling the angled end of sample holders with barium sulphate paste. The paste was pressed against a smooth surface and left to dry. This formed a surface of known reflectance mounted with the same geometry used for fabric measurements. Therefore, it was assumed that the response of the sphere was held constant between calibration and measurement. The corresponding transmission reference is simply an open tube. Again, by calibrating with an open sample holder in place it was assumed that the response of the sphere was held constant between calibration and measurement.

Rotatable Sample Holder

Transmission measurements were also made without the integrating sphere. A rotatable sample holder made from a piece of aluminium plate and a graduated dial enabled beam-beam transmittance measurements over a wide range of incidence angle. The aluminium plate had an aperture where the fabric sample could be mounted. The incident beam was simply aligned with the detector such that scattered radiation was excluded.

Fabric Samples

A wide variety of drapery fabrics were obtained with the primary aim of selecting individual samples that fit into each designation described by Keyes (1967). Samples were found for all designations except IIID. A sheer fabric was added to the set. Sheer fabrics do not fall into any of the customary designations. The thickness of fabric samples ranged from 0.1 to 1.0 mm. (0.004 to 0.04 in.). Measurements at normal incidence were made and specular reflection was not detected in any fabric sample.

Photographs of the fabric samples are shown in Figure 5 and more specific details regarding the samples are listed in Table 1.

Transmittance Measurement

With the reflection port closed a transmittance reference, a fixed sample holder without any sample attached, was

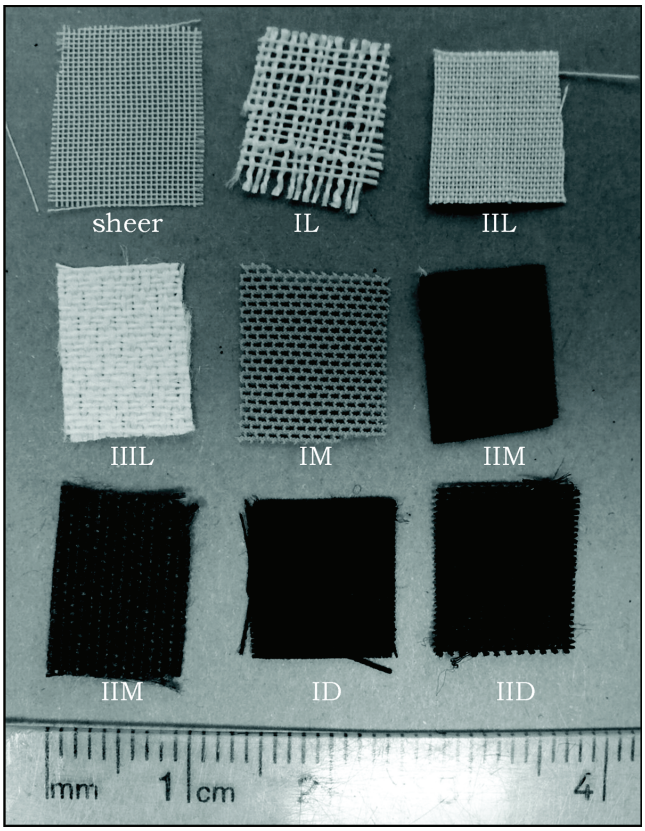

Figure 5 *Photograph of fabric test samples (refer to Table 1).*

mounted at the transmission port. The 100% baseline readings were taken. The transmission port was blocked and the 0% baseline readings were taken.

A fabric sample was attached to the angled end of the sample holder and mounted at the transmission port as shown in Figure 6a. With the reflection port closed, spectral readings were taken to obtain τ_{bt}^{m}. The reflection port was opened and τ_{bd}^{m} readings were taken. The 0% and 100% baseline calibration data were applied to the spectral transmittance readings using Equation 1 (ASTM, E903-96 1996) producing spectral transmission measurements.

$$\tau(\lambda) = \frac{S_\lambda - Z_\lambda}{F_\lambda - Z_\lambda} \quad (1)$$

S_λ is the unadjusted spectrophotometer reading. Z_λ and F_λ are the 0% and 100% baseline readings taken at the same wavelength.

Equation 1 was also applied to transmission readings made without the integrating sphere. In this configuration τ_{bb}^{m} was measured at θ equal to $15^\circ, 30^\circ, 45^\circ, 60^\circ, 70^\circ$ and 80°. Baseline readings were taken for 0% and 100% transmission by blocking the beam and by leaving the beam unobstructed, respectively.

Table 1. Characteristics of Fabric Test Samples

Fabric Colour	Fabric Designation	Weave Type	Yarn Count	
			Warp	Filling
Cream	sheer	Plain weave	74	74
White (1)	IL	Plain weave	40	40
White (2)	IIL	Plain weave	76	129
White (3)	IIIL	Dobby weave	60	60
Green	IIM	Plain weave	78	116
Blue	IIIM	Plain weave	40	88
Black (2)	IID	Plain weave	76	120
			Wale	Course
Black fabric (1)	ID	Warp knit	30	30
Brown	IM	Warp knit	20	17

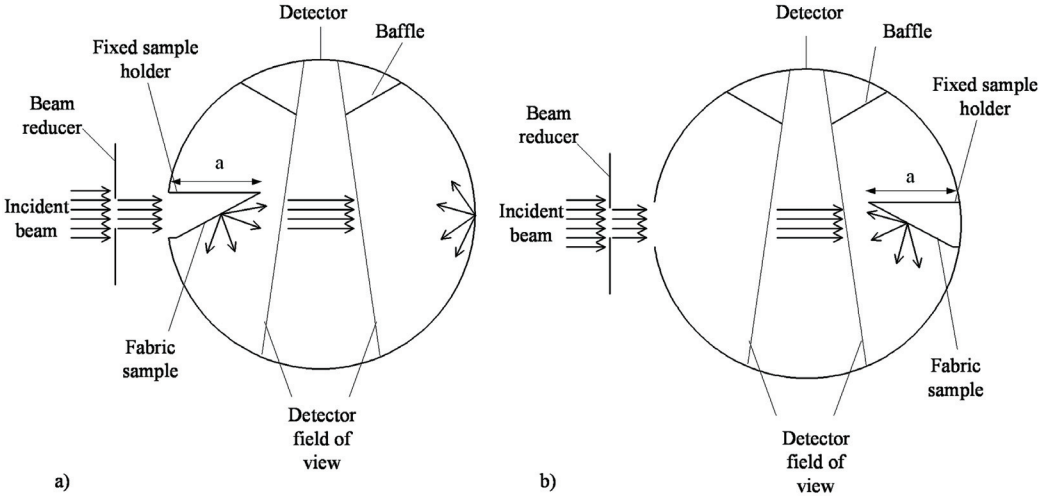

Figure 6 *Integrating sphere measurements with fixed sample holders: a) Transmittance measurement; b) Reflectance measurement.*

Reflectance Measurements with the Integrating Sphere

A reflectance reference with an end angle θ was installed at the reflection port. The transmission adapter was installed at the transmission port to reduce the size of the incident beam. The 100% baseline was recorded. The reflectance reference was replaced with an open sample holder (same θ) and the 0% baseline was recorded.

A fabric sample was attached to the angled end of the sample holder and mounted at the reflection port as shown in Figure 6b. Spectral beam-diffuse reflectance readings were taken.

Calculation of Solar Properties

Having obtained the measurements of interest, the solar optical properties were calculated using the 50-point selected ordinate method described in ASTM E903-96 (1996). The solar spectrum (ASTM E891-87 1987) was divided into 50 equal-energy wavelength intervals. For example, τ_{bb}^{m} was calculated as:

$$\tau_{bb}^{m} = \frac{1}{50} \sum_{i=1}^{50} \tau_{bb}^{m}(\lambda_i) \tag{2}$$

where λ_i is the wavelength at the centre of the i^{th} spectral interval.

Measurement Uncertainty

Uncertainty in integrating sphere measurements may be attributed to several factors and these are documented in ASTM E903-96 (1996). The uncertainty associated with the raw measurements, with or without the integrating sphere, is very small. The spectrophotometer was configured and multiple samples were taken for each reading such that the uncertainty attached to spectral readings was well below 1% (95% confidence level). More significant uncertainty is associated with the conversion of spectral data to solar properties. Uncertainty caused by choice of solar spectrum was ignored. The uncertainty in the transmittance and reflectance measurements using the integrating sphere was estimated to be ±0.03 while the uncertainty in the beam-beam transmittance measurements made without the integrating sphere was ±0.02. Error bars representing this uncertainty are shown on the IL and ID beam-total transmittance data shown in Figure 11.

The technique used to achieve off-normal incidence raised questions about bias errors that might arise. However, these bias errors were generally eliminated by calibration. Comments regarding three possible sources of error are included in the following subsections.

Using Barium Sulphate as the Reflectance Standard

The solar reflectance of barium sulphate, used as a reflectance standard in this study, was measured and found to be 2% lower than the reflectance of the PTFE reflectance standard that is customarily used with the integrating sphere. The software supplied with the spectrophotometer applies Equation 1 as if the PTFE is present. Therefore, a 2% correction was applied to adjust (downward) the solar reflectance measurements made when barium sulphate was used for calibration.

Reduction of the Incident Beam

Preliminary investigation showed that measurements were in error by about 2% because the fixed sample holder tubes were intercepting a small portion of the incident beam. Reduction of the incident beam eliminated this error.

Projection of Sample Holder into the Integrating Sphere

Typical configurations for transmittance and reflectance measurements using a fixed sample holder are shown in Figure 6. In each case the sample holder projected into the sphere at a distance a = 40 mm. (a = 1.57 in.). Preliminary measurements, with a sample holder inserted at different distances, showed that the response of the sphere changed by about 3% at most. (Little difference was noted between similar experiments conducted using polished tubes, unpolished tubes and tubes coated with barium sulphate.) This error was eliminated by calibrating the integrating sphere prior to each experiment with the sample holder in place.

Orientation of the Sample Holder

Calibration and measurements were completed with the angled end of the sample holder facing downward as shown in Figure 6. This was done to be sure that the detectors could not directly view the test sample. However, bias error arises in the case of diffuse transmission measurements because the scattered radiation originating at the sample is not distributed uniformly over the surface of the integrating sphere and the radiation sensed by the detectors includes the first reflection of this non-uniform distribution. Using the assumption that the radiation scattered by the fabric is diffuse, theory can be used to evaluate a correction factor that is a function of only geometry and the reflectance of the sphere. The correction factor tends to unity as the fabric sample is moved closer to the wall of the sphere or as the reflectance of the sphere approaches unity. For the conditions that apply to this study the adjustment is so small, a small fraction of one percent, that it was not applied. Theory also shows that the calibration procedure eliminates this source of error in the fabric reflection measurements.

SEMI-EMPIRICAL MODELS

Defining Apparent Yarn Reflectance

Consider the reflection of solar radiation at normal incidence.

$$\rho_{bt}^{m}(\theta = 0) = \rho_{bb}^{m}(\theta = 0) + \rho_{bd}^{m}(\theta = 0) \tag{3}$$

However, $\rho^m_{bb}(\theta = 0) = 0$, so

$$\rho^m_{bt}(\theta = 0) = \rho^m_{bd}(\theta = 0) \tag{4}$$

In order to make an approximate distinction between yarns of different colors (i.e., different solar reflectivity) we define an apparent yarn reflectance, ρ^y. This is done by noting that reflection arises only from the portion of the material that intercepts radiation, $(1 - A_o)$. Thus, the following expression was used to establish a definition of ρ^y.

$$\rho^m_{bd}(\theta = 0) = \rho^y \cdot (1 - \tau^m_{bb}(\theta = 0)) = \rho^y \cdot (1 - A_o) \tag{5}$$

or,

$$\rho^y = \frac{\rho^m_{bt}(\theta = 0)}{1 - A_o} \tag{6}$$

The apparent yarn reflectance was found to be useful in the development of the off-normal reflectance model.

Beam-Beam Transmittance Model

Values of τ^m_{bb} measured without the integrating sphere were plotted with respect to θ. See Figure 7. The maximum value of τ^m_{bb} is found at θ = 0 and τ^m_{bb} decreases as θ increases, approaching zero for most fabrics near θ = 80°.

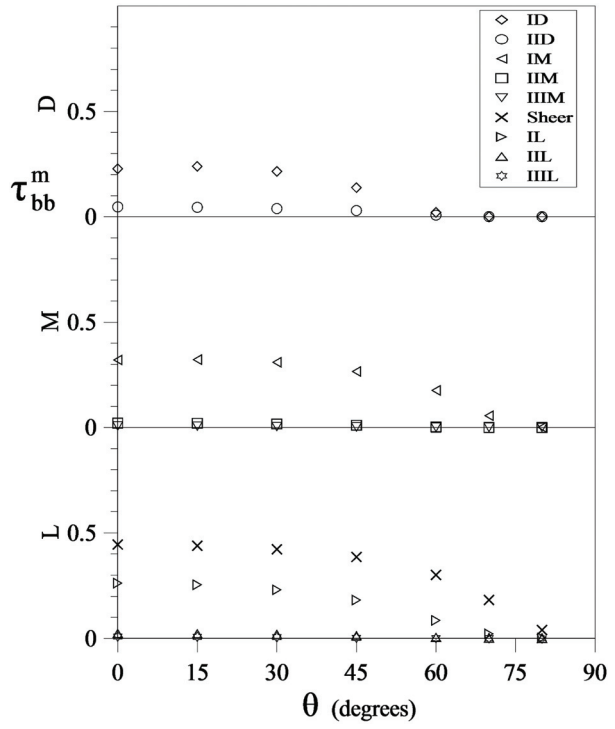

Figure 7 *Beam-beam transmittance versus incidence angle (from measurements without integrating sphere).*

Comparing the τ^m_{bb} measurements made with and without the integrating sphere no appreciable difference was found. The two sets of $\tau^m_{bb}(\theta = 0)$ can be found in Table 2 and a comparison for samples with discernable transmission values (category I, open-weave fabrics) is shown in Table 3. Generally, discrepancies between the two sets of measurements (diff) did not exceed the stated uncertainty. Beam-beam transmittance results from the integrating sphere were expected to be less reliable because they are obtained by taking the difference between two other measurements but no difficulty was encountered. The observed agreement strengthens the credibility of the measurements made using the fixed sample holders. At this stage the τ^m_{bb} values made without the integrating sphere were set aside and models were developed using only the data measured using fixed sample holders installed in the integrating sphere.

Beam-beam transmission measurements were normalized according to Equation 7.

$$^{norm}\tau^m_{bb} = \frac{\tau^m_{bb}(\theta)}{\tau^m_{bb}(\theta = 0)} \tag{7}$$

Measured values of $^{norm}\tau^m_{bb}$ are shown as data points in Figure 8. It was assumed that the normalized data points could be represented by the function shown in Equation 8. Curves produced with various values of the exponent, b, are also shown in Figure 8.

$$^{norm}\tau^m_{bb} = \frac{\tau^m_{bb}(\theta)}{\tau^m_{bb}(\theta = 0)} = \cos^{\,b}(\theta) \tag{8}$$

Using Figure 8 a value of the exponent b was assigned to each fabric while recognizing the importance of greater accuracy at intermediate values of θ. The off-normal adjustment should and will have little influence at small values of θ. This is true by default because the cosine function is used. Considerable leeway is available at large values of θ because the incident flux falls to zero as θ approaches 90°. Also take note of the two data points plotted near the upper left corner of Figure 8, the open circle and square. These points can safely be disregarded because they correspond to fabrics with very little beam-beam transmission. In other words, if $\tau^m_{bb}(\theta = 0)$ is small the value of b will have almost no influence on the value of $\tau^m_{bb}(\theta)$ produced by the model. Because priorities of this type cannot easily be expressed in a mathematical sense, many of the parameters evaluated in the development of these models were assessed by eye.

Examining Figure 8, the relationship between the exponent b and fabric properties is not immediately apparent. Recognizing that values of $\tau^m_{bb}(\theta)$ must be the same for the front and back surfaces of the fabric a correlation was sought based on the only input parameter that is free of front/back influence; the openness, $A_o = \tau^m_{bb}(\theta = 0)$. Figure 9 shows a plot of data points for b, estimated using Figure 8, versus openness. Equation 9, also shown in Figure 9, can be used to estimate values of the exponent, b.

Table 2. Summary of Measured Solar Optical Property Measurements at Normal Incidence

		Measurement with Integrating Sphere				Measurement without Integrating Sphere
Fabric Color	Fabric Designation	Beam-Total Reflectance	Beam-Total Transmittance	Beam-Diffuse Transmittance	Beam-Beam Transmittance	Beam-Beam Transmittance
Cream	Sheer	0.19	0.80	0.36	0.44	0.45
White (1)	IL	0.42	0.56	0.32	0.24	0.26
White (2)	IIL	0.56	0.43	0.42	0.01	0.01
White (3)	IIIL	0.68	0.30	0.29	0.01	0.01
Brown	IM	0.23	0.64	0.30	0.34	0.33
Green	IIM	0.32	0.28	0.26	0.02	0.02
Blue	IIIM	0.38	0.20	0.19	0.01	0.01
Black (1)	ID	0.15	0.32	0.12	0.20	0.23
Black (2)	IID	0.21	0.23	0.18	0.05	0.05

Table 3. Comparison Between Beam-Beam Transmittance Measurements with and without Integrating Sphere (IS)

	ID			IM			IL		
Incidence Angle (deg)	with IS	without IS	Diff	with IS	without IS	Diff	with IS	without IS	Diff
0	0.23	0.20	0.03	0.32	0.33	-0.01	0.26	0.24	0.02
15	0.23	0.19	0.04	0.32	0.33	-0.01	0.25	0.24	0.01
30	0.21	0.18	0.03	0.31	0.32	-0.01	0.23	0.23	0.0
45	0.14	0.11	0.03	0.27	0.27	0.0	0.18	0.18	0.0
60	0.02	0.01	0.01	0.18	0.19	-0.01	0.09	0.11	-0.02

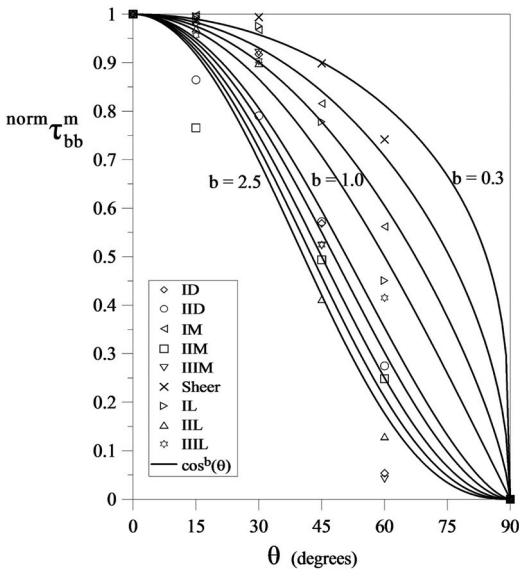

Figure 8 *Normalized beam-beam transmittance versus incidence angle (from measurements with integrating sphere).*

$$b = Max\left\{-\frac{1}{2}\ln(Max\{\tau_{bb}(\theta = 0), 0.01\}), 0.35\right\} \quad (9)$$

Rearranging Equation 8,

$$\tau^m_{bb}(\theta) = \tau^m_{bb}(\theta = 0) \cdot \cos^{\,b}(\theta) \quad (10)$$

where b is given by Equation 9 and $\tau^m_{bb}(\theta = 0)$ is measured or can be equated to A_o.

Ideally, Equation 9 would have been formulated in such a way that b approaches zero as $A_o = \tau^m_{bb}(\theta = 0)$ approaches unity. In this limit the fabric disappears and Equation 10 applies no off-normal adjustment. However, some compromise was needed in order to maintain the simplicity of the model while ensuring that the calculated absorptance of the fabric does not fall below zero for all possible input values.

The data points shown in Figure 10 represent the measured values of $\tau^m_{bb}(\theta)$ and the lines represent Equation 10.

Beam-Total Transmittance Model

The measured values of τ^m_{bt} were plotted against θ. See Figure 11.These plots show a gradual decrease in τ^m_{bt} from its maximum value at θ = 0 as θ increases. Recognizing that τ^m_{bb} may decrease more sharply than τ^m_{bt} with respect to θ it was anticipated that the diffuse transmission component, τ^m_{bd}, might increase with θ. Values of τ^m_{bd} were plotted. See Figure 12. In fact, the measured values of τ^m_{bd} show little variation with θ over the range of measurement.

Having obtained no measurements beyond θ = 60° the value of $\tau^m_{bd}(\theta = 90°)$ is not known. This presents difficulty in the development of a correlation. However, by examining the trends of τ^m_{bt}, and also by recognizing that there is some leeway for approximation at high values of θ, it was assumed that

$$\tau^m_{bt}(\theta = 90°) = \tau^m_{bd}(\theta = 90°) = 0 \quad (11)$$

Equation 12 was used to normalize τ^m_{bt}.

$$^{norm}\tau^m_{bt} = \frac{\tau^m_{bt}(\theta)}{\tau^m_{bt}(\theta = 0)} \quad (12)$$

The normalized data points were represented by a function of the form:

$$^{norm}\tau^m_{bt} = \cos^{\,b}(\theta) \quad (13)$$

Again, values of the exponent b were assessed while recognizing the importance of greater accuracy at intermediate values of θ and the following expression, almost identical to Equation 9, was developed.

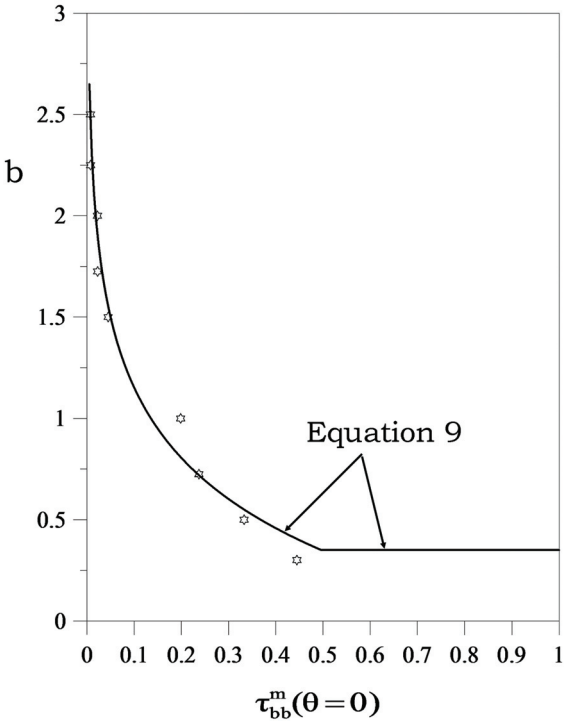

Figure 9 *Exponent b versus $\tau^m_{bb}(\theta = 0)$, for Equation 10.*

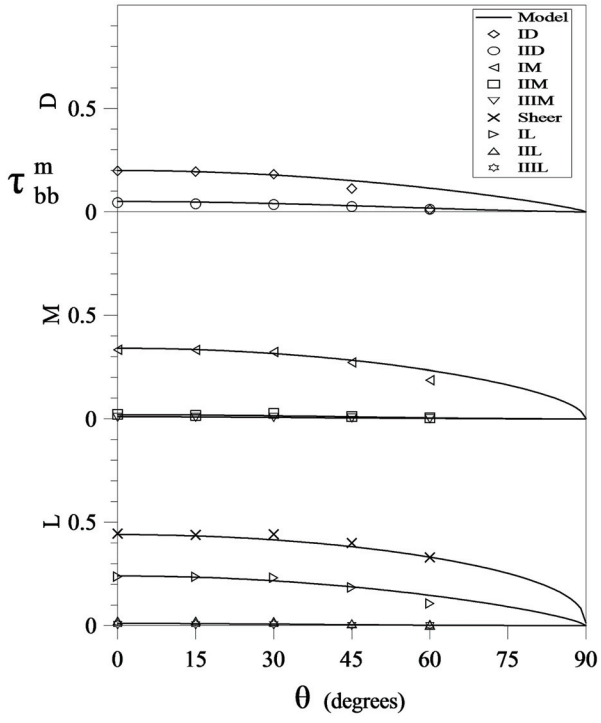

Figure 10 *Beam-beam transmittance versus incidence angle.*

$$b = Max\left\{-\frac{1}{2}\ln(Max\{\tau_{bt}(\theta = 0), 0.01\}), 0.35\right\} \quad (14)$$

Rearranging Equations 12 and 13,

$$\tau_{bt}^{m}(\theta) = \tau_{bt}^{m}(\theta = 0) \cdot \cos^{b}(\theta) \quad (15)$$

The curves shown in Figure 11 represent Equation 15.

Beam-Diffuse Transmittance Model

At any given value of θ, τ_{bd}^{m} is the difference between τ_{bt}^{m} and τ_{bb}^{m}.

$$\tau_{bd}^{m}(\theta) = \tau_{bt}^{m}(\theta) - \tau_{bb}^{m}(\theta) \quad (16)$$

The curves shown in Figure 12 represent Equation 16.

Beam-Total Reflectance Model

Measured values of ρ_{bt}^{m} are shown in Figure 13. As expected, ρ_{bt}^{m} increases with θ but the increase is gradual and $\rho_{bt}^{m}(\theta = 90°)$ could not be measured. Recall that $\rho_{bt}^{m} = \rho_{bd}^{m}$. Observing that $\rho_{bt}^{m}(\theta)$ does not change appreciably over the range of θ used for measurements it was assumed that:

$$\rho_{bt}^{m}(\theta = 90°) \neq 1 \quad (17)$$

Noting that all of the incident radiation will strike the yarn, regardless of the degree of openness, as θ approaches 90° an expression was sought to evaluate $\rho_{bt}^{m}(\theta = 90°)$ as a function of yarn reflectance, ρ^{y}. Equation 18 was developed by approximately extrapolating the measurements of fabric reflectance at values of θ up to 60°.

$$\rho_{bt}^{m}(\theta = 90°) = \rho_{bt}^{m}(\theta = 0)(1 - \rho_{bt}^{m}(\theta = 0)) \cdot (0.7(\rho^{y})^{0.7}) \quad (18)$$

The normalized beam-total reflectance is

$$^{norm}\rho_{bt}^{m} = \frac{\rho_{bt}^{m}(\theta) - \rho_{bt}^{m}(\theta = 0)}{\rho_{bt}^{m}(\theta = 90°) - \rho_{bt}^{m}(\theta = 0)} \quad (19)$$

The measured values of $^{norm}\rho_{bt}^{m}$ were found to fit a function of the form

$$^{norm}\rho_{bt}^{m} = 1 - \cos^{b}(\theta) \quad (20)$$

In this case the value of the exponent b can be taken as a constant.

$$b = 0.6 \quad (21)$$

Finally, rearranging Equations 19 and 20,

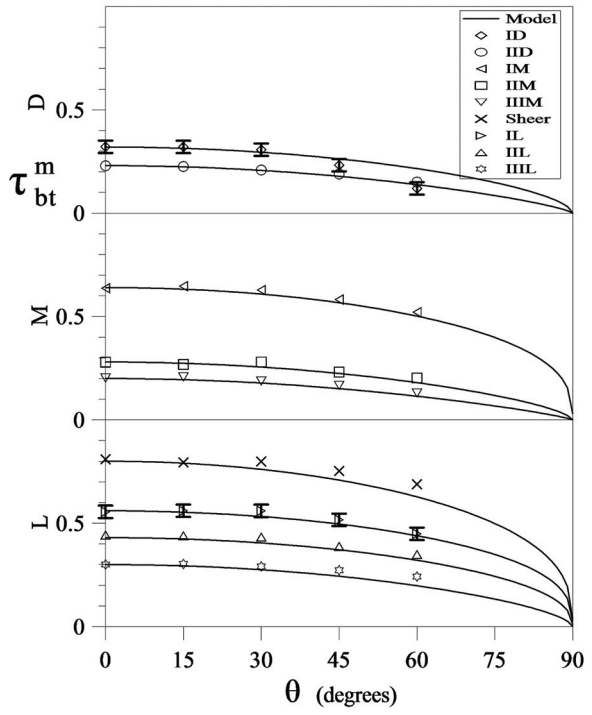

Figure 11 *Beam-total transmittance versus incidence angle.*

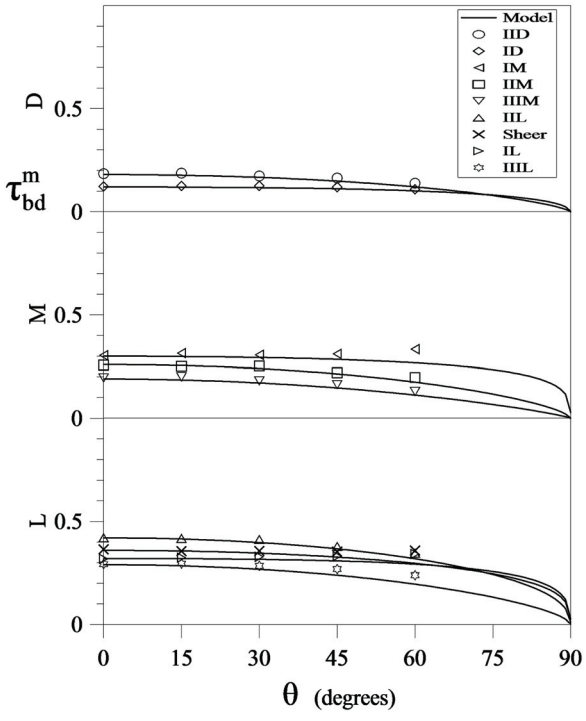

Figure 12 *Beam-diffuse transmittance versus incidence angle.*

$$\rho_{bt}^{m}(\theta) = \rho_{bt}^{m}(\theta = 0) + (\rho_{bt}^{m}(\theta = 90°) - \rho_{bt}^{m}(\theta = 0)) \cdot (1 - \cos^{b}(\theta)) \quad (22)$$

The curves plotted in Figure 13 represent Equation 22.

Diffuse-Diffuse Transmittance and Reflectance Models

The solar optical properties for incident diffuse radiation can be obtained by integrating the beam-total properties over the hemisphere. The diffuse-diffuse transmittance is

$$\tau_{dd}^{m} = 2\int_{0}^{\pi/2} \tau_{bt}^{m}(\theta) \cdot \cos(\theta) \cdot \sin(\theta) d\theta \quad (23)$$

Similarly, the diffuse-diffuse reflectance is:

$$\rho_{dd}^{m} = 2\int_{0}^{\pi/2} \rho_{bt}^{m}(\theta) \cdot \cos(\theta) \cdot \sin(\theta) d\theta \quad (24)$$

Equations 23 and 24 can readily be evaluated numerically.

DISCUSSION

The white fabrics fall in the light (L) colour designation while the black fabrics fall in the dark (D) colour designation.

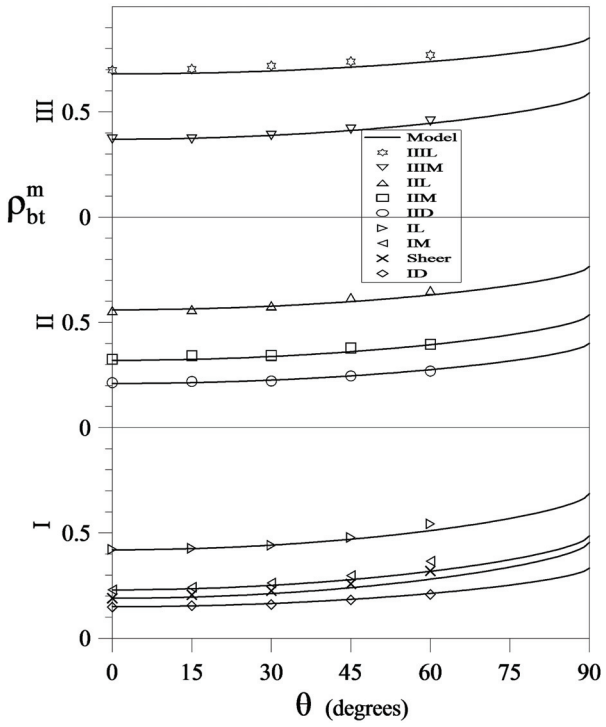

Figure 13 *Beam-total reflectance versus incidence angle.*

The brown, the green and the blue fabrics all fall in the medium (M) colour designation. The cream sheer fabric with a very high τ_{bt}^{m} falls outside the range of Keyes' chart. For each colour designation, the open weave (I) fabrics have the lowest ρ_{bt}^{m}. This is expected because, for a given type of yarn, closed weave fabrics have the greatest surface area exposed to the incident radiation. On the other hand, the open weave fabrics have the highest τ_{bt}^{m} followed by the semi-open weave fabrics while the closed weave fabrics (III) exhibit the lowest τ_{bt}^{m} in each colour designation.

Comparisons between integrating sphere measurements and the semi-empirical models are shown in Figures 10 to 13. Generally, the models agree very well with the measurements. Only the open weave fabrics (IL, IM, ID) show appreciable discrepancy. In this case τ_{bb}^{m} in particular would benefit from the use of a cutoff angle but this option was not used for the sake of retaining simplicity – knowing that more leeway regarding accuracy is available as θ approaches 90°.

Viewing Figures 10 through 13, the overriding observation is that the proposed models agree very closely with almost all of the measurements. It is also worth noting that in practice the evaluation of off-normal solar properties using these models will be influenced most strongly by the corresponding solar properties measured at normal incidence. The models presented here represent adjustments that will have little influence at small values of θ because the cosine function was used for each formulation. Also the correlations will have little importance at large values of θ, the situation for which few measurements were available and more uncertainty is present, because the incident flux approaches zero. Measured data were available for the intermediate values of θ, the situation where accuracy is most important, and the correlations are expected to work well in this range.

Finally, it is worth noting that the fabric test samples used in this study did not have different front- and back-surface properties. However, the correlations have been formulated in such a way that they can be applied to fabrics that do differ front-to-back and are expected to also work well in this situation. This claim is made because the data required as input will include the front and back solar properties measured at normal incidence and these properties will most directly convey the influence of front/back differences whether these differences are appreciable or not. Remember that A_o and $\tau_{bb}^{m}(\theta)$ are functions of fabric/yarn geometry only, albeit on a very fine scale, and their front/back values must be equal.

CONCLUSIONS

A novel technique has been developed to measure the off-normal solar optical properties of drapery fabrics. The research involved the design and fabrication of special sample holders that were attached to an integrating sphere that is used in conjunction with a spectrophotometer. This apparatus was designed to measure solar optical properties at normal incidence. Measurements were then taken at varying incidence angles for a wide variety of fabrics. It was found that solar

properties at off-normal incidence, including beam and diffuse components, can be predicted on the basis of corresponding properties measured at normal incidence. Correlations were formulated by fitting a cosine power function to the measured data. The proposed models offer significant value for computing the effective solar properties of pleated drapes/curtains in the context of building energy simulation and in fact these models have been used to examine the effective solar properties of pleated drapes (Kotey et al. 2009).

In general, the agreement between integrating sphere measurements and the resulting correlations was remarkably good. However, some discrepancy was noted with respect to the beam-beam transmission of open weave fabrics at high incidence angle. If greater accuracy is desired it is recommended that the models developed in the current study be re-evaluated using a larger set of fabric samples in a set of measurements that extend to a higher range of incidence angle.

ACKNOWLEDGEMENTS

Financial support from the Natural Sciences and Engineering Research Council (NSERC) and ASHRAE is gratefully acknowledged. We are also grateful for the assistance of Prof. Maureen Grasso (University of Georgia) and the diligence of Charles Barnaby (Wrighsoft Corporation).

NOMENCLATURE

A_o = openness
F = full scale baseline
L = light-colored
M = medium-colored
S = spectrophotometer reading
Z = zero baseline
b = exponent in semi-empirical models

Roman Numerals

I = open weave
II = semi-open weave
III = closed weave

Greek Letters

λ = wavelength
ρ = reflectance
τ = transmittance
θ = incidence angle

Subscripts

bb beam-beam
bd beam-diffuse
bt beam-total
dd diffuse-diffuse
λ spectral

Superscripts

m fabric property
norm normalized property
y yarn property

REFERENCES

ASHRAE. 2005. ASHRAE Handbook-Fundamentals. Atlanta: American Society of Heating Refrigeration and Air Conditioning Engineers, Inc.

ASTM E891-87. 1987. Standard Tables for Terrestrial Direct Normal Solar Spectral Irradiance for Air Mass 1.5. Philadelphia: American Society for Testing and Materials.

ASTM E903-96. 1996. Standard Test Method for Solar Absorptance, Reflectance, and Transmittance of Materials Using Integrating Spheres. Philadelphia: American Society for Testing and Materials.

Edwards, D.K, Gier, J.T., Nelson, K.E. and R.D. Roddick. 1961. Integrating sphere for imperfectly diffuse samples. Applied Optics, 51: 1-12

Farber, E.A., Smith, W.A., Pennington, C.W., and J.C. Reed. 1963. Theoretical analysis of solar heat gain through insulating glass with inside shading. ASHRAE Journal, pp. 79.

Furler, R.A. 1991. Angular dependence of optical properties of homogeneous glasses. ASHRAE Transactions, 97 (2): 1129-1133.

Hunn, B.D., Grasso, M.M., Beaudry, M.A., and P.J. House. 1991. Measurement of bidirectional solar optical properties of shading fabrics. ASHRAE Transactions, 97: 455-464.

Karlsson, J., and A. Roos. 2000. Modelling the angular behavior of the total solar energy transmittance of windows. Solar Energy, 69(4): 321-329.

Keyes, M.W. 1967. Analysis and rating of drapery materials used for indoor shading. ASHRAE Transactions, 73, (1): 8.4.1.

Klems, J.H. 1994a. A new method for predicting the solar heat gain of complex fenestration system – 1. Overview and derivation of the matrix layer calculation. ASHRAE Transactions, 100(1): 1065-1072.

Klems, J.H., 1994b. A new method for predicting the solar heat gain of complex fenestration system – 2. Detailed description of the matrix layer calculation. ASHRAE Transactions, 100(1): 1073-1086.

Kotey, N.A., Wright, J.L. and Collins, M.R., 2007, A simplified method for calculating the effective solar optical properties of a drapery. Proceedings of the 32nd Conference of the Solar Energy Society of Canada Inc. (SESCI) and 2nd Conference of the Solar Building Research Network (SBRN), Calgary, Alberta, Canada, June 9-13, 2007.

Kotey, N.A., Collins, M.R., Wright, J.L., and T. Jiang. 2008. A simplified method for calculating the effective solar optical properties of a venetian blind layer for building

energy simulation. Accepted for Publication in ASME Journal of Solar Energy Engineering.

Kotey, N.A., Wright, J.L., Collins, M.R., 2009, A Detailed Model to Determine the Effective Solar Optical Properties of Draperies, ASHRAE Transactions, Vol. 115, Pt. 1.

Lovell, D.J. 1984. Theory and applications of integrating sphere technology. Laser Focus/Electro-Optics. May 1984: 86-96

Moore, G.L., Pennington, C.W., 1967, Measurement and application of solar properties of drapery shading materials, ASHRAE Transactions Vol. 73, Pt. 1

Parmelee, G. V. and W.W. Aubele., 1952, The shading of sunlit glass: an analysis of the effect of uniformly spaced flat opaque slats. ASHVE Transactions, 58: pp. 377-398.

Pettit, R.B. 1979. Hemispherical transmittance properties of solar glazings as a function of averaging procedure and incident angle. Solar Energy Materials, 1: 125-140.

Pfrommer, P., Lomas, K.J., Seale, C., and Chr. Kupke. 1995. The radiation transfer through coated and tinted glazing. Solar Energy, 54(5): 287-299.

Pfrommer, P., Lomas, K.J., and Chr. Kupke.1996. Solar radiation transport through slat-type blinds: A new model and its application for thermal simulation of buildings. Solar Energy. 57(2): 77-91

Roos, A. 1997. Optical characterization of coated glazings at oblique angles of incidence: Measurements versus model calculations. Journal of Non-Crystalline Solids, 218: 247-255.

Rubin, M., Von Rottkay, K., and R. Powles. 1998. Models for the angle-dependent optical properties of coated glazing. Solar Energy, 66(4): 267-276.

Rubin, M., Von Rottkay, K., and R. Powles. 1999. Window optics. Solar Energy, 62(3): 149-161.

van Dijk, H., Kenny, P., and J. Goulding. (eds), 2002. WIS – Advanced Windows Information System – Reference Manual.

Wright, J.L., and N.A. Kotey. 2006. Solar absorption by each element in a glazing/shading layer array. ASHRAE Transactions, 112(2): 3-12.

Wright, J.L., 2008, "Calculating Centre-Glass Performance Indices of Glazing Systems with Shading Devices," ASHRAE Transactions, Vol. 114, Pt. 2.

Yahoda, D.S. and J.L. Wright. 2005. Methods for calculating the effective solar-optical properties of a venetian blind layer. ASHRAE Transactions, 111(1): 572-586.